PHYSICAL REVIEW C, VOLUME 65, 025503

Muon capture by ^{11}B and the hyperfine effect

V. Wiaux,* R. Prieels, J. Deutsch, and J. Govaerts
Université catholique de Louvain, B-1348 Louvain-la-Neuve, Belgium

V. Brudanin and V. Egorov
Joint Institute for Nuclear Research, RU-141980 Dubna, Russia

C. Petitjean
Paul Scherrer Institute, CH-5232 Villigen, Switzerland

P. Truöl
University of Zürich, CH-8057 Zürich, Switzerland

(Received 7 September 2001; published 23 January 2002)

This paper reports a precision measurement of the ratio of the exclusive capture rates from the two hyperfine levels of the muonic ^{11}B atom leading to the excited level of ^{11}Be at 320 keV: $\lambda^+/\lambda^- = 0.028 \pm 0.021$(stat.) ± 0.003 (syst.). Using the most up-to-date halo wave functions of the nuclei involved, the induced pseudoscalar to axialvector form factor ratio is obtained as $g_P/g_A = 4.3^{+2.8}_{-4.3}$(stat.) ± 0.5 (syst.). This value agrees with the partial conservation of the axial current prediction and does not reproduce the anomaly observed in radiative muon capture on hydrogen. The hyperfine conversion rate between the two hyperfine levels is also determined, $R = [181 \pm 16(\text{stat.}) \pm 1(\text{syst.})] \times 10^3\ \text{s}^{-1}$. The total capture rate from the lower hyperfine level and its difference compared to the upper one were also determined: $\lambda_C^- = [23.53 \pm 0.72(\text{stat.}) \pm 0.25(\text{syst.})] \times 10^3\ \text{s}^{-1}$ and $\Delta\lambda = [-13.2 \pm 1.7(\text{stat.}) \pm 0.7(\text{syst.})] \times 10^3\ \text{s}^{-1}$.

DOI: 10.1103/PhysRevC.65.025503 PACS number(s): 23.40.−s, 29.90.+r, 12.38.Qk, 12.15.Ji

I. INTRODUCTION

In the electroweak standard model (SM), nuclear muon capture results from capture on a *u* quark, namely, the reaction

$$\mu^- + u \rightarrow \nu_\mu + d. \tag{1.1}$$

Generally however, the process may be described at the nucleon level through form factors parametrizing the Lorentz invariant effective Hamiltonian (e.g., Ref. [1]),

$$H_{\text{eff}} = \frac{G_F}{\sqrt{2}} V_{ud} J_l^{\mu\dagger} J_\mu^h + \text{H.c.} \tag{1.2}$$

with

$$\frac{G_F}{\sqrt{2}} = \frac{g^2}{8M_W^2}, \quad J_l^\mu = \overline{\psi}_\mu \gamma^\mu (1-\gamma_5)\psi_\nu, \tag{1.3}$$

and

$$J_h^\mu = V_h^\mu - A_h^\mu, \tag{1.4}$$

$$V_h^\mu = \overline{\psi}_n \left[g_V(q^2)\gamma^\mu + i\frac{g_M(q^2)}{2M}\sigma^{\mu\nu}q_\nu \right] \psi_p, \tag{1.5}$$

$$A_h^\mu = \overline{\psi}_n \left[g_A(q^2)\gamma^\mu\gamma^5 + \frac{g_P(q^2)}{m_\mu} q^\mu \gamma^5 \right] \psi_p. \tag{1.6}$$

Our notations for form factors are standard; *g* stands for the basic $SU(2)_L$ gauge coupling constant at tree-level, M_W is the mass of the charged intermediate vector boson, V_{ud} is the relevant Cabibbo-Kobayashi-Maskawa matrix element, and *M* is the average nucleon mass.

In the above parametrization, second-class currents are ignored, since they are expected to provide a negligible contribution [3]. The remaining four quantities $g_i(q^2)$ are the first-class nucleon electroweak form factors taken at the value of the invariant momentum transfer q^2 of the reaction. Three of these form factors are known with good precision [1,2]. The induced pseudoscalar one, however, $g_P(q^2)$, is not determined to the same level of accuracy and has been the object of numerous investigations through muon capture both on the proton and on nuclei, of which the experiment reported in this note is a specific instance.

Partial conservation of the axial current (PCAC) as well as spontaneous chiral symmetry breaking in the strong interactions vacuum implies that the dominant contribution to g_P is provided by muon capture on a virtual pion which couples to the axial current [1,2]. Hence, g_P is related to the pion decay constant f_π and the pion-nucleon coupling $g_{\pi NN}$. At the momentum transfer relevant to muon capture on the proton, this relation implies the value $g_P = 8.6$. More recent QCD-based evaluations predict the interval $g_P = 8.23 - 8.46$ [4,5].

Nuclear muon capture is generally described in the impulse approximation, namely, by assuming capture on free

---

*Present address: IMEC, Belgium.

nucleons, while their nuclear binding is accounted for through the use of nuclear wave functions optimized to fit various observables [1]. This method however, may suffer significant corrections in the case of the induced pseudoscalar coupling g_P since both the pion decay constant and pion-nucleon coupling are modified in the nuclear medium, and perhaps the pion mass and thus its propagator may also be influenced by pion interactions with its surroundings. This possibility has raised much interest in relation to quark condensation at high nuclear densities, but recent investigations do not confirm the expected spectacular effects in actual nuclear conditions as originally predicted [6,7].

The induced pseudoscalar coupling has recently witnessed a great revival of interest since the value extracted from a radiative muon capture experiment on hydrogen [8] exceeds the theoretical expectation by about 50% [9]. Presently available results from ordinary muon capture on hydrogen are not of sufficient accuracy to confirm or invalidate this situation (see, for instance, the review in Ref. [2]), thus justifying new high precision measurements in preparation [10].

The issue of coupling and mass renormalizations through nuclear medium effects has been studied using both rate and correlation measurements in ordinary muon capture, and rate measurements alone in radiative ones. In ordinary muon capture, the most reliable and precise result has been reached in the very light ^{3}He nucleus and is in good agreement with the unrenormalized PCAC prediction [11]. Results for ^{12}C, ^{16}O, and ^{23}Na present some scatter but do not display any strong deviation from predictions [2]. Finally, recent results in ^{28}Si indicate a possible quenching of the pseudoscalar interaction in this nucleus [12].

In radiative muon capture (RMC), there seems to be a tendency for g_P to decrease with increasing A [13]. In various nickel isotopes the RMC yield seems also to decrease with increasing A [14], but this effect may find an explanation through other causes than a modification of g_P [14,15]. The issue remains unsettled as yet.

In view of this situation we undertook anew the experimental determination of g_P through the observation of the hyperfine effect in the exclusive capture of muons in ^{11}B yielding the 320 keV excited state of ^{11}Be.

In nuclei of nonzero spin the ground-state of the muonic atom has two hyperfine levels which feature two different capture rates [16]. If a hyperfine transition between these two levels occurs because of an Auger effect [17], the capture product and the electron decay time distributions present a deviation from a pure exponential, which depends on the hyperfine populations, the hyperfine conversion rate as well as the muon capture rates from the two levels.

The effect was observed for the first time in ^{19}F [18] and Delorme stressed the sensitivity of the partial capture rates to g_P [19]. In 1968, Grenacs emphasized the interest of observing an exclusive reaction of the type considered in this note and a first experiment was performed [20].

Assuming the population of the two hyperfine levels for the μ^{11}B atom to be initially statistical [21], namely, with $N_0^+ = 5/8$ for the upper and $N_0^- = 3/8$ for the lower levels, the appearance rates of the decay electrons and of the 320 keV photons are

$$\frac{dN_{\text{electrons}}}{dt} = N_0^+ \lambda_0 e^{-\lambda_D^- t}\left[\left(\frac{N_0^-}{N_0^+} + \frac{R}{R+\Delta\lambda}\right) + \left(1 - \frac{R}{R+\Delta\lambda}\right) e^{-(R+\Delta\lambda)t}\right], \tag{1.7}$$

$$\frac{dN_{\gamma_{320}}}{dt} = N_0^+ \lambda^- e^{-\lambda_D^- t}\left[\left(\frac{N_0^-}{N_0^+} + \frac{R}{R+\Delta\lambda}\right) + \left(\frac{\lambda^+}{\lambda^-} - \frac{R}{R+\Delta\lambda}\right) e^{-(R+\Delta\lambda)t}\right]. \tag{1.8}$$

In these expressions, λ_0 stands for the positive muon decay rate, λ_D^- for the muon disappearance rate from the lower hyperfine level, R for the Auger conversion rate between these upper and lower levels, and $\Delta\lambda$ for the difference between the total capture rates from the two levels. Finally, the two quantities of primary interest to us, λ^+ and λ^-, are the exclusive capture rates to the 320 keV hyperfine level of ^{11}Be from the two hyperfine levels of the mesic ^{11}B state. The sensitivity of the ratio λ^+/λ^- to g_P was first evaluated by Bernabeu [22]. Given the 1/2 spin value of the final state, it is easily seen that the capture rate from the upper ($F=2$) hyperfine level would be vanishing were it not for the contribution of the induced pseudoscalar coupling and d-wave neutrino emission.

The expression (1.8) also displays the sensitivity of the γ appearance rate to the hyperfine effect, provided the hyperfine conversion rate R allows its observation during the muon lifetime. A determination of the rate R by μSR techniques provided the value $(3.3\pm0.5)\times10^5\ \text{s}^{-1}$ [23] comfortably close to the mean muon disappearance rate of $(4.771\pm0.007)\times10^5\ \text{s}^{-1}$ [24] in ^{11}B.

In the following, the experimental lay-out which allowed us to observe the time evolution of the 320 keV γ ray is described. The observation of the time evolution of the decay electrons, required for the determination of the other parameters which enter expressions (1.7) and (1.8), is also addressed.

II. EXPERIMENTAL SETUP

The aim of the experimental setup is to measure the following two distributions: on the one hand, the energy and time distribution of γ rays subsequent to nuclear muon capture, and on the other hand, the time distribution of the muon decay electrons emitted by the sample of exotic atoms μ^{11}B. The setup is illustrated in Fig. 1.

The experiment was performed in the $\mu E4$ area at the Paul Scherrer Institute (PSI, Switzerland), exposing the target to the muon beam of 49.1 MeV/c in its chromatic mode, characterized by its high momentum resolution: $\Delta P/P = 3\%$ (FWHM). This good resolution reduces range straggling and thus minimizes muon stops in materials other than boron. The target consists of a PVC cup filled with a high purity (99.999%) natural boron powder of submicron grain size, having a density $\rho = 524\ \text{mg/cm}^3$. Two circular mylar

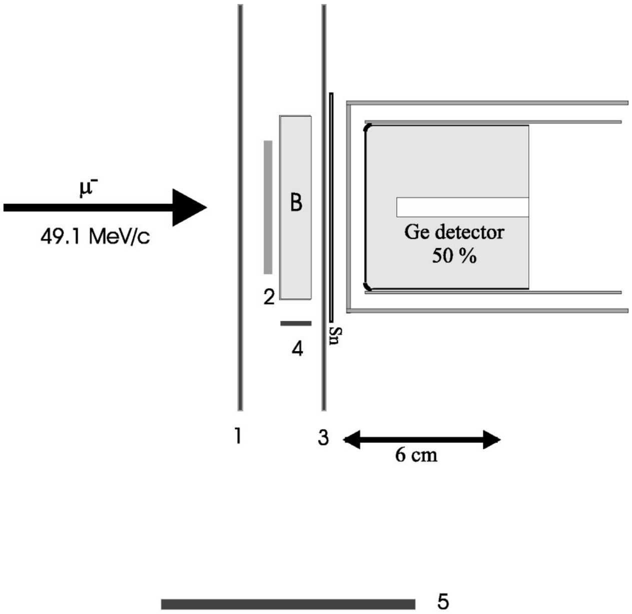

FIG. 1. Schematic view of the experimental setup.

windows of 175 μm seal the PVC box on both sides. The inner diameter of the box is 72 mm and the thickness of the boron target is 12 mm. The stop distribution was estimated through Monte Carlo simulations to be 3 mm FWHM.

The target is surrounded by two plastic scintillators (S_1 and S_2) upstream and another one (S_3) downstream. While all muons leaving the beam pipe are detected by S_1, the detector S_2 selects only those entering the central part of the target (diameter: 52 mm). Its use rejects muon capture events in the PVC ring surrounding the boron powder. Anticoincidence with the third detector S_3 defines the muon stop (μstop) in the target: $S_1 \cdot S_2 \cdot \overline{S_3}$. A 50% HPGe detector, placed downstream along the beam axis, observes the γ rays which leave the target in that direction and measures their energy. A 1 mm thick Sn shield, placed between the S_3 scintillator and the HPGe detector, absorbs the low energy muonic x rays whose pile-up could affect the time evolution at the 320 keV line. A telescope of two additional scintillators ($S_4 \cdot S_5$) detects the decay electrons leaving the target laterally.

III. DATA STRUCTURE

The mean rate of μstops is 9×10^3 s^{-1}. If it has not been preceded by another muon in S_1 during the previous 10 μs, a μstop opens a 10 μs observation window. A time to digital converter (TDC) measures in bins of 1.25 ns the time between the beginning of that window and its coincidence with a γ ray in the HPGe detector or an electron in the $S_4 \cdot S_5$ telescope. In order to avoid that the uncorrelated background affects the time distribution of the correlated events, an updated dead-time of 12 μs is triggered by any Ge or $S_4.S_5$ signal.

The γ ray coincidences that are retained as good events meet the following criteria.

(i) One requires that no ‘‘second muon’’ $\mu_{\rm sec}$ (signal of muon in S_1) has arrived during the 10 μs window.

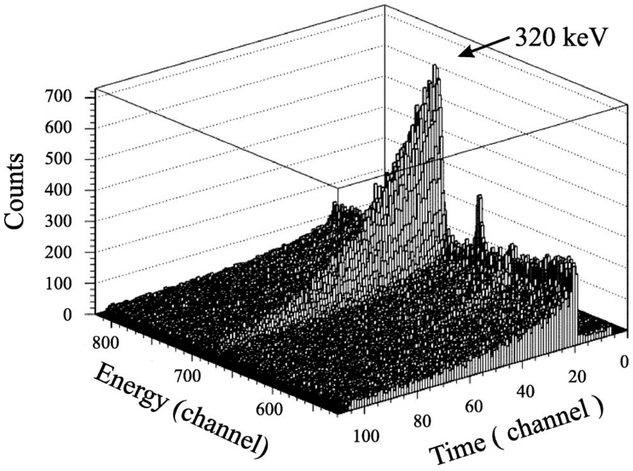

FIG. 2. Two dimensional energy-time spectrum. The 320 keV γ line is clearly dominating over the smooth time dependent background. The time is given in 100 ns per channel. Energy calibration is given by the relation $E(\text{keV}) = -8.675 + 0.478$ channel.

(ii) Any signal in coincidence with S_1 or S_3 is rejected as a potential bremsstrahlung event.

(iii) A retained γ ray event should be detected in a ‘‘quiet’’ HPGe detector: one requires the absence of any γ rays preceding the signal within 20 μs, as well as the absence of any Michel electron in the HPGe detector for the previous 120 μs.

(iv) The detection of a γ ray in the HPGe detector and that of a decay electron in the $S_4 \cdot S_5$ telescope during the 10 μs window also results in the rejection of those γ candidates.

Those γ ray events which pass all these selection criteria are then recorded in a two dimensional energy-time histogram (see Fig. 2).

Electron events defined as coincidences in $S_4 \cdot S_5$ in the 10 μs window are selected as good events in the absence of any second muon $\mu_{\rm sec}$; in the absence of any spurious electron signal in S_1 or S_3; and in the absence of any γ ray detected in the HPGe detector. Those events which pass these rejection criteria are recorded in a one-dimensional time histogram (see Fig. 3).

IV. THE ANALYSIS

A. The background

The time evolution of the γ ray emission rate from ^{11}Be* is extracted from the first histogram, energy versus time. This requires the knowledge of the time evolution of the background in the energy bin defined at 320 keV. Consequently, the time evolution in energy bins to the left and to the right of the 320 keV bin must also be considered. An energy and time dependent function $bkg(E,t)$, describing this background, is constrained by the fit to the time spectra corresponding to each of the selected energy bins. The energy bins used for the determination of the background time evolution and their contents relative to the 320 keV line are shown in Fig. 4 after an integration over 10 μs.

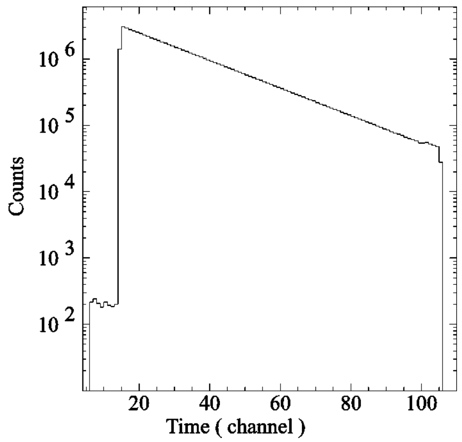

FIG. 3. Time spectrum of the electrons detected in the lateral telescope. The time is given in 100 ns per channel. The region between channels 15 and 96 is used for the fit.

B. The response function

The combined time-response function of the detector and of the electronics is extracted from a measurement of muonic x rays at 296.4 and 372.5 keV with a Mg target. Since these are emitted for each atomic muon capture, they are prompt and dominate the spectrum, while the observed function of time thus correctly reflects the response function. The time behavior of these two lines is corrected for a smooth time dependent subtraction of the background taken every 1.25 ns on both sides in energy of each line. The normalization of the two resulting time spectra leads to the time response functions $f_{296}(t)$ and $f_{372}(t)$, at 296.4 and 372.5 keV, respectively. For each time bin, a linear interpolation between those two functions then gives the time response function $f_E(t)$ at any energy E within that interval

$$f_E(t)=f_{296}(t)+[f_{372}(t)-f_{296}(t)]\left(\frac{E-296.4}{372.5-296.4}\right). \tag{4.1}$$

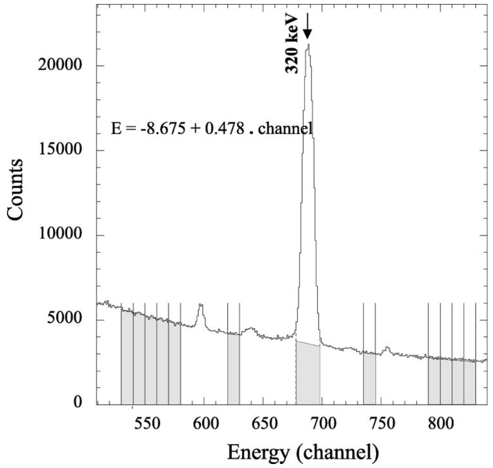

FIG. 4. Gamma energy distribution integrated over 10 μs. The shaded areas delimited by vertical lines indicate the selected windows used in the background determination.

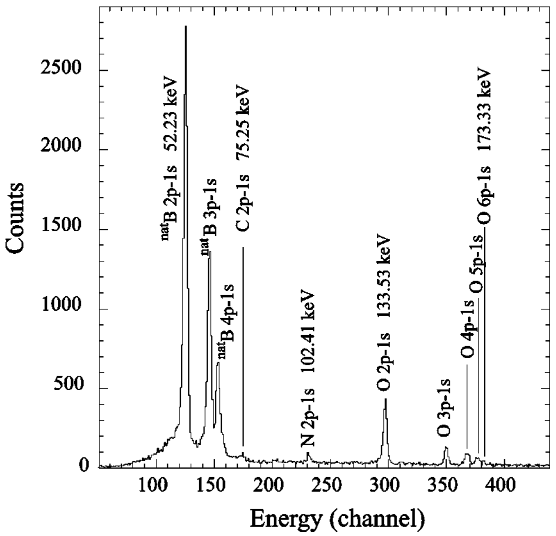

FIG. 5. Gamma energy distribution of muonic x rays integrated over 300 ns.

This function is then used to convolute the time dependence of the 320 keV line given in Eq. (1.8).

C. The electron spectrum

As discussed before, the fit of the decay electron spectrum constrains some useful parameters such as λ_D^- and $\Delta\lambda$. However, the capture of muons by residual impurities, in the target and its surroundings, adds some background to that spectrum. The analysis of the relative abundancies of muonic x rays from K transitions leads to the identification and the evaluation of the contribution from each of the impurity elements (see Fig. 5). In order to deduce the impurity content of our target, the germanium detector was exposed without the Sn shield so that x-ray lines emitted in the atomic capture process could be observed. In order to maintain a good signal-to-noise ratio, only the first 300 ns following a muon stop were considered.

The number of x-rays detected must be corrected for their yield and the photopeak detection efficiency in the HPGe detector. The HPGe efficiency between 50 and 200 keV is deduced from a combination of measurements with calibrated radioactive sources and simulations. The simulations use the GEANT software (version 3.21, CERN), and require a precise description of the detector geometry as well as of the μstop distribution within the target. Comparison of simulations with efficiency measurements using calibrated pointlike ^{133}Ba and ^{152}Eu sources leads to a precise determination of the detector geometry. The comparison of simulations with the measurements of the abundancies of the ^{11}B x-rays as a function of the beam momentum, as well as the knowledge of the transverse profile of the beam [25], leads to the description of the μstop distribution within the target.

Electrons from the μ^{10}B state provide the main component of the physical electron background: 24.54±0.26% normalized to the ^{11}B contribution. This admixture results from the use of a natural boron target. Enriched targets tested turned out not to have the required chemical purity. Just as

TABLE I. Values of the free parameters resulting from the fit to the data, with $\chi^2/N_{\mathrm{DF}}=1154/1085=1.064$.

	λ^+/λ^-	R (10^3 s^{-1})	λ_D^- (10^3 s^{-1})	$\Delta\lambda$ (10^3 s^{-1})
Results	0.028	181	478.70	-13.2
Statistical error	± 0.021	± 16	± 0.72	± 1.7
Systematic error	± 0.003	± 1	± 0.25	± 0.7

for ^{11}B, the time distribution of electrons emitted by mesic ^{10}B is affected by the hyperfine effect, following the expression (1.7) with the appropriate values for the various parameters

$$N_0^+(^{10}\mathrm{B})=8/14,\quad N_0^-(^{10}\mathrm{B})=6/14,$$
$$R(^{10}\mathrm{B})=2.1(5)\times10^5\ \mathrm{s}^{-1}[23], \tag{4.2}$$

$$\lambda_D^-(^{10}\mathrm{B})=482.9+[\lambda_D^-(^{11}\mathrm{B})-477.1]\pm1.0\times10^3\ \mathrm{s}^{-1}, \tag{4.3}$$

$$\Delta\lambda(^{10}\mathrm{B})=[\Delta_{\mathrm{rel}}(^{10}\mathrm{B})\lambda_C^-(^{10}\mathrm{B})]/[1-\Delta_{\mathrm{rel}}(^{10}\mathrm{B})N_0^+(^{10}\mathrm{B})], \tag{4.4}$$

with for Eq. (4.4)

$$\lambda_C^-(^{10}\mathrm{B})=\lambda_D^-(^{10}\mathrm{B})-\lambda_0,$$

$$\Delta\lambda(^{10}\mathrm{B})=\lambda_C^+(^{10}\mathrm{B})-\lambda_C^-(^{10}\mathrm{B}),$$

$$\Delta_{\mathrm{rel}}(^{10}\mathrm{B})=\Delta\lambda(^{10}\mathrm{B})/\langle\lambda_C\rangle(^{10}\mathrm{B})=-0.98^{+0.10}_{-0.05}, \tag{4.5}$$

where $\langle\lambda_C\rangle(^{10}\mathrm{B})$ and $\lambda_C^-(^{10}\mathrm{B})$ are the mean capture rate and the capture rate from the lower hyperfine level in ^{10}B, respectively. Let us comment on the two parameters $\lambda_D^-(^{10}\mathrm{B})$ and $\Delta\lambda(^{10}\mathrm{B})$.

The mean disappearance rates of $(482.9\pm0.7)\times10^3$ s^{-1} in ^{10}B and of $(477.9\pm0.7)\times10^3$ s^{-1} in ^{11}B are given by Suzuki [24]. However, the analysis of the measurements reported in that paper does not take into account the hyperfine effect. As a result, the reported mean disappearance rate underestimates the disappearance rate from the lower hyperfine level λ_D^-. We assume in Eq. (4.3) that this underestimation is identical for both boron isotopes, since the transition rate R and the hyperfine effect $\Delta\lambda$ are similar for both isotopes. Any small difference between the transition rates R of both boron isotopes has a negligible effect on this correction.

Finally, the hyperfine effect on the total capture rates in ^{10}B is deduced in Eq. (4.4) from the theoretical expectation for the ratio $\Delta\lambda(^{10}\mathrm{B})/\langle\lambda_C\rangle(^{10}\mathrm{B})$ in ^{10}B [18,24,26] using the g_P value predicted by PCAC. The errors on $\Delta_{\mathrm{rel}}(^{10}\mathrm{B})$ given in Eq. (4.5) correspond to a dependence on g_P in the conservative range of $0<g_P/g_A<14$. We assumed that the dependence of $\Delta_{\mathrm{rel}}(^{10}\mathrm{B})$ on g_P in ^{10}B is similar to the one in ^{11}B which was evaluated by Koshigiri *et al.* in Ref. [27]. We included this variation into our systematic error evaluation. In any case the impact of this assumption on the final error of our results is negligible.

Other contributions to the background in the electron spectrum stem from O $(6.38\pm0.34\pm0.20\%)$, and to a lesser degree, from N $(0.45\pm0.06\pm0.01\%)$ and C $(0.43\pm0.10\pm0.01\%)$. The appearance of oxygen in the target is possibly due to the oxidation of the boron powder as well as to humidity. These contributions follow exponential time distributions with known lifetimes [24]. Finally, noncorrelated events are described by a constant rate and determined from their contributions at negative times. The time response function for the electron spectrum was neglected since it is much smaller than the 100 ns channel width taken in the electron spectra.

D. The fit

The theoretical functions were adjusted simultaneously to the γ and electron spectra. For the γ spectra, the convoluted background function $\mathrm{bkg}(E,t)\otimes f_E(t)$ in various energy bins, summed with the convoluted signal evolution of the 320 keV peak $dN_{320}/dt(t)\otimes f_{320}(t)$ was used. For the electrons, the signal time evolution $dN_{e^-}/dt(t)$ was added to the evolution of the background in the manner described above.

Even though the four parameters of main interest λ_D^-, $\Delta\lambda$, R, λ^+/λ^- influence both the electron and the γ time evolutions, the electron time spectrum constrains essentially the total lower disappearance rate λ_D^- and the difference between the upper and lower capture rates $\Delta\lambda$. As for the time evolution of the 320 keV γ ray, it constrains essentially the hyperfine conversion rate R and the ratio of exclusive capture rates λ^+/λ^-. The remaining free parameters are those of the background energy and time evolution, and of the normalizations of the electron and γ signals.

Minimization used the MINUIT software (version 96.03, CERN), which adjusts the theory to the data by a least-square method. The fit converges to the results presented in Table I, with $\chi^2/N_{\mathrm{DF}}=1154/1085$.

The 1σ statistical error on each value presented in Table I results from the quadratic sum of the error given by MINUIT and that of the contributions induced by the statistical errors on the fixed parameters of the fit. Among the latter, the dominant one is the error on $R(^{10}\mathrm{B})$ whose relative contribution in quadrature to the final error on λ^+/λ^- is less than 1%. Data statistics remains the major source of error. The systematic error is the sum of the contributions due to the systematic errors on the fixed parameters of the fit.

The quality of the fit is displayed in Fig. 6, which presents the fit of a Gaussian function to the residual distributions $[\equiv(\mathrm{data}-\mathrm{theory})/\sigma]$ for the 320 keV γ spectrum, the electron spectrum, and the background energy and time γ spectrum.

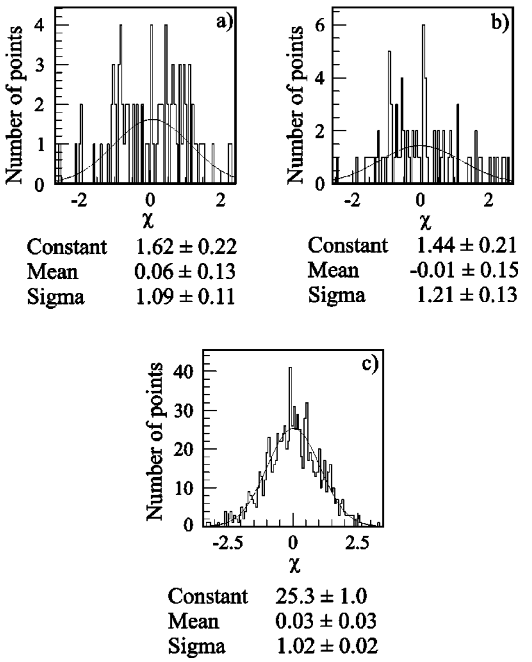

FIG. 6. Distribution of weighted residuals (data-theory)/σ for (a) the 320 keV γ time distribution, (b) for the electron time distribution, and (c) for the smooth background time and energy distribution.

The quality of the fit to the γ and electron data is further illustrated in Figs. 7 and 8. In each case, the upper plot shows the residual (data-theory/σ) in each time channel. The lower one shows the time evolution of the signal after subtraction of the background $dN_{320}(t)/dt$ or $dN_{e^-}(t)/dt$, divided by the pure exponential $e^{-\lambda_D^- t}$ with λ_D^- provided by the fit (Table I). These figures display a nice illustration of the hyperfine effect and of the hyperfine conversion. Preferential feeding of the lower hyperfine state, from which the capture mainly occurs, is clearly observed both in the γ and electron time spectra. However the amplitude of the effect is enhanced in the γ spectrum by the hyperfine effect on the partial capture rates.

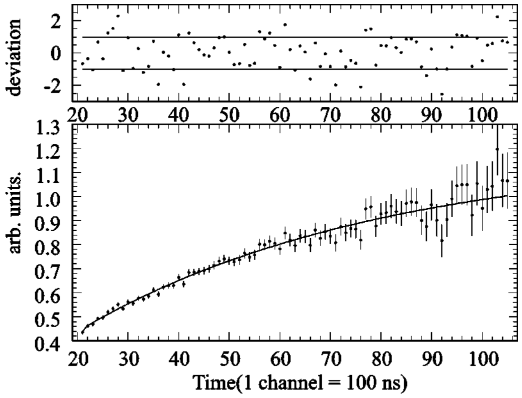

FIG. 7. Upper part: distribution of weighted residuals (data theory)/σ per point for the 320 keV γ time distribution. Lower part: time evolution of the 320 keV γ after background subtraction and divided by a pure exponential.

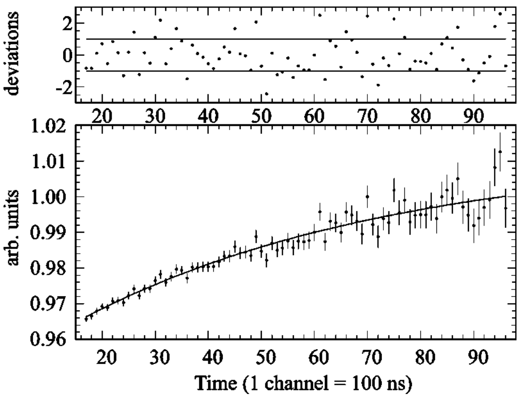

FIG. 8. Upper part: distribution of weighted residuals (data-theory)/σ per point for the electron time distribution. Lower part: time evolution of the electron after background subtraction and divided by a pure exponential.

V. DISCUSSION OF THE RESULTS

A. Various secondary results

Before we consider the main result of this experiment, namely, the ratio λ^+/λ^- giving access to the value of the induced nucleon pseudoscalar coupling g_P in ^{11}B, let us discuss some of the interesting secondary results obtained. In the present experiment, the hyperfine conversion rate is determined with a 10% precision, which is much better than that of previous experiments [20,23]

$$R=(181\pm16\pm1)\times10^3\ \ \mathrm{s}^{-1}, \tag{5.1}$$

and is in reasonable agreement with the early theoretical expectation $R=250\times10^3\ \ \mathrm{s}^{-1}$ of Ref. [18]. Our measured conversion rate is significantly lower than the one reported in Ref. [23] [$R=(330\pm50)\times10^3\ \ \mathrm{s}^{-1}$], leading to a sensitivity of the experiment to g_P poorer than originally expected on the basis of that value. If not statistical, this 3 σ discrepancy with our result, may hint at specific relaxation phenomena in the experiment of Ref. [23] due to solid-state effects. Indeed, this latter experiment used the transverse field muon spin rotation technique, studying the residual polarized population of the hyperfine levels. The fast disappearance of muon precession observed from the upper hyperfine component may be due in part to magnetic relaxation phenomena triggered by a random static internal field which would have the same signature as muon hyperfine conversion. Indeed, such a relaxation was observed for positive muons in ^{11}B [29].

Another side-result is a new value for the muon disappearance rate λ_D^-

$$\lambda_D^-=(478.70\pm0.72\pm0.25)\times10^3\ \ \mathrm{s}^{-1}, \tag{5.2}$$

slightly larger than the earlier values reported in Ref. [24], and the references quoted therein. All former values available in the literature [24,28] result from analyses which ignore both the hyperfine effect and hyperfine conversion. Since nuclear muon capture is favored from the lower hyperfine level, this unwarranted approximation leads to an underestimation of λ_D^-. Our result was determined without any

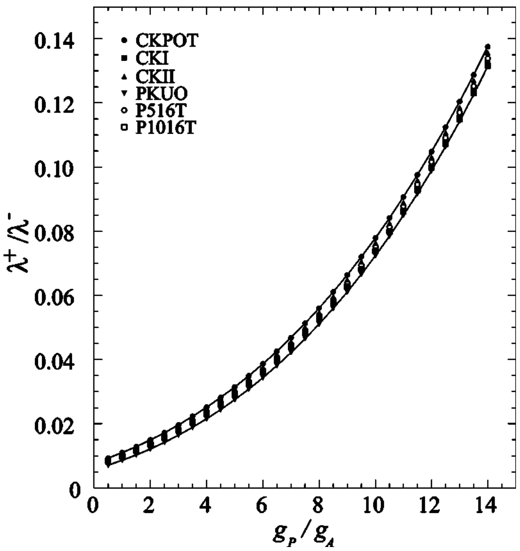

FIG. 9. Theoretical predictions for λ^+/λ^- as a function of g_P/g_A for various nuclear models. Definitions may be found in Ref. [30].

approximation, using in our fits the entire complexity of the hyperfine process [see Eqs. (1.7) and (1.8)]. This value 5.2 yields the total muon capture rate from the lower hyperfine level,

$$\lambda_C^- = \lambda_D^- - \lambda_0 = (23.53 \pm 0.72 \pm 0.25) \times 10^3 \ \ \mathrm{s}^{-1}, \quad (5.3)$$

in reasonable agreement with the theoretical expectation of $\lambda_C^- = 20.6 \times 10^3 \ \ \mathrm{s}^{-1}$ [27].

For the difference between the total capture rates for the two hyperfine levels we obtain

$$\Delta\lambda = \lambda_C^+ - \lambda_C^- = (-13.2 \pm 1.7 \pm 0.7) \times 10^3 \ \ \mathrm{s}^{-1}. \quad (5.4)$$

This first ever measured value is to be compared to the prediction of $\Delta\lambda = -9.9 \times 10^3 \ \ \mathrm{s}^{-1}$ [27].

B. The main result and the resulting constraint on g_P/g_A

As reported in Table I, the ratio of the exclusive capture rates λ^+ and λ^- which we studied takes the value

$$\frac{\lambda^+}{\lambda^-} = 0.028 \pm 0.021(\mathrm{stat.}) \pm 0.003(\mathrm{syst.}), \qquad (5.5)$$

which is an important improvement over the only existing limit, $\lambda^+/\lambda^- \leqslant 0.26$ [20]. The precision on λ^+/λ^- in this type of experiment could be improved using muonic atoms with larger hyperfine conversion rates than in ^{11}B.

The sensitivity of this ratio to the induced nucleon pseudoscalar coupling in ^{11}B was first evaluated in Ref. [22]. More recently Kuzmin *et al.* [30] evaluated this sensitivity including various recoil-order corrections and considering all the $(0p)$ states for the protons and neutrons outside the closed ^{4}He core. Assuming spherical harmonic oscillator wave functions and various residual interactions to determine the configuration mixing, these authors find a good stability of the variation of λ^+/λ^- as a function of g_P/g_A. From Fig. 9, one notices the small scatter among the predictions derived from various plausible configuration mixings.

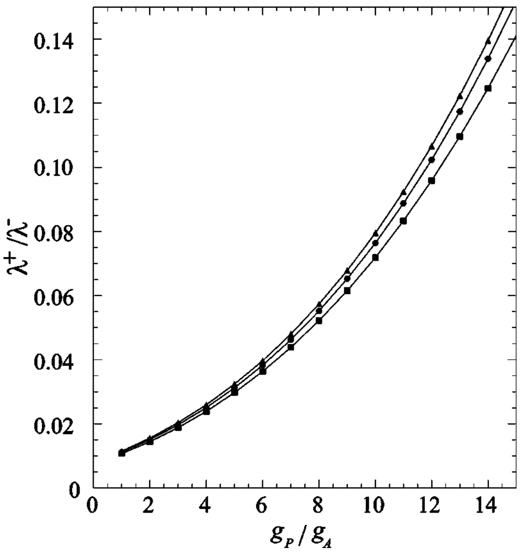

FIG. 10. Theoretical predictions for λ^+/λ^- as a function of g_P/g_A, for harmonic oscillator wave functions: circles (CKPOT [30]); and for Woods-Saxon potential: squares (spherical) [31]; or triangles (deformed) [32].

The evaluation of Ref. [30] assumes identical spherically symmetric harmonic oscillator potentials both for ^{11}B and ^{11}Be. This may be questioned given the small binding energy (183 keV) of the neutron in the final state of the nuclear capture process. Consequently, its wave function cannot be expected to be well described by a harmonic oscillator well of the same radius as that of the capturing proton in ^{11}B. It is indeed well known that ^{11}Be is a typical "neutron halo"

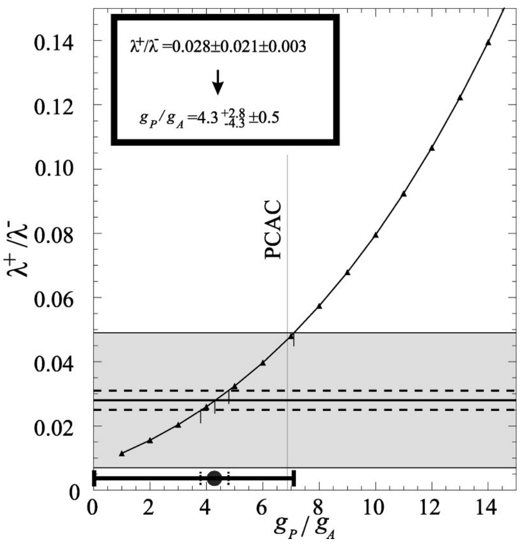

FIG. 11. Theoretical predictions for λ^+/λ^- as a function of g_P/g_A given by the CKPOT shell model [30]. The neutron halo is described by a deformed Woods-Saxon potential [31,32]. The horizontal full lines indicated the 1σ statistical error on λ^+/λ^- while the dashed lines indicates the systematic error.

nucleus [33,34]. This feature was taken into account in Ref. [31] and—as a further refinement—Ref. [32] also introduced a deformation into the Woods-Saxon potential which both these theoretical works used.

The effect of these two modifications is displayed in Fig. 10 by comparing it to the most plausible prediction (CKPOT) of Ref. [30]. Some variation is observed but it remains small in comparison to our experimental error. It may be noted that absolute values of capture rates may also be determined using these three theoretical approaches, which seems to favor that of Ref. [30].

In conclusion, we may combine our experimental result with the most elaborate theoretical evaluation [32]. This is done in Fig. 11 which indicates that our experiment is in agreement—even though with sizeable error bars—with the PCAC-based prediction, leading to the result

$$\frac{g_P}{g_A}=4.3^{+2.8}_{-4.3}(\text{stat.})\pm 0.5(\text{syst.}). \tag{5.6}$$

In particular, we see no indication of an enhancement in the value for g_P, in contradistinction to what has been observed in radiative muon capture on hydrogen [8] and possibly in light nuclei [13].

ACKNOWLEDGMENTS

We are grateful to V.A. Kuzmin and to L. Grenacs for many valuable discussions and to T. Suzuki for having provided us with his results before publication. We would also like to thank the Technical University of Munich and J. Hartman for the loan of HPGe detectors, as well as the Paul Scherrer Institute for excellent beam conditions and financial support.

---

[1] N. C. Mukhopadhyay, Phys. Rep. **30**, 1 (1977).
[2] V. Wiaux, Ph.D. thesis, 1999, Catholic University of Louvain, available at URL http://www.fynu.ucl.ac.be/librairie/theses
[3] H. Shiomi, Nucl. Phys. **A603**, 281 (1996).
[4] V. Bernard, L. Elouadrhiri, and U.-G. Meissner, hep-ph/0107088; V. Bernard *et al.*, Phys. Rev. D **50**, 6899 (1994).
[5] H. W. Fearing *et al.*, Phys. Rev. D **56**, 1783 (1997).
[6] J. Delorme and M. Ericson, Phys. Rev. C **49**, 1763 (1994).
[7] J. Delorme *et al.*, Nuovo Cimento **102**, 273 (1976), and references quoted therein.
[8] G. Jonkmans *et al.*, Phys. Rev. Lett. **77**, 4512 (1996); D. H. Wright *et al.*, Phys. Rev. C **57**, 373 (1998).
[9] V. Bernard, T. R. Remmert, and U.-G. Meissner, Nucl. Phys. **A686**, 290 (2001), and references therein.
[10] Cl. Petitjean *et al.*, PSI Experiment No. R-97-05.2.
[11] P. Ackerbauer *et al.*, Phys. Lett. B **407**, 224 (1998).
[12] C. Briançon *et al.*, Nucl. Phys. **A671**, 647 (2000); see also S. Ciechanowicz *et al.*, nucl-th/0105061.
[13] P. C. Bergbusch *et al.*, Phys. Rev. C **59**, 2853 (1999), and Table IV therein.
[14] T. P. Gorringe *et al.*, Phys. Rev. C **58**, 1767 (1998).
[15] H. W. Fearing and M. S. Welsh, Phys. Rev. C **46**, 2077 (1992).
[16] J. Bernstein *et al.*, Phys. Rev. **111**, 313 (1958).
[17] R. Winston and V. L. Telegdi, Phys. Rev. Lett. **7**, 104 (1961).
[18] R. Winston, Phys. Rev. **129**, 2766 (1963).
[19] J. Delorme, Nuovo Cimento **32**, 1360 (1964).
[20] J. P. Deutsch *et al.*, Phys. Lett. **28B**, 178 (1968).
[21] J. G. Congleton, Phys. Rev. A **48**, R12 (1993).
[22] J. Bernabeu, Nuovo Cimento A **4**, 715 (1971).
[23] D. Favart *et al.*, Phys. Rev. Lett. **25**, 1348 (1970).
[24] T. Suzuki *et al.*, Phys. Rev. C **35**, 2212 (1987).
[25] Cl. Petitjean (private communication).
[26] H. Primakoff, Rev. Mod. Phys. **31**, 802 (1959).
[27] K. Koshigiri *et al.* Prog. Theor. Phys. **71**, 1293 (1984).
[28] M. Eckhause *et al.*, Phys. Rev. **132**, 422 (1963).
[29] V. Wiaux, UCL internal report, 1994.
[30] V. A. Kuzmin *et al.*, Phys. At. Nucl. **57**, 1881 (1994).
[31] T. Suzuki, Proceedings of the International Symposium on Non-Nucleonic Degrees of Freedom Detected in the Nucleus, 1996, Osaka, Japan (unpublished).
[32] D. Ridikas and J. S. Vaagen, ECT* Report No. ECT*-96-006, 1996; see also R. Ridikas *et al.*, Nucl. Phys. **A609**, 21 (1996); R. Ridikas *et al.*, *ibid.* **A628**, 363 (1998).
[33] R. Anne *et al.*, Phys. Lett. B **304**, 55 (1993).
[34] R. Anne *et al.*, Nucl. Phys. **A575**, 125 (1994).